Disrupted Brain Connectivity Networks in Drug-Naive, First-Episode Major Depressive Disorder

Junran Zhang, Jinhui Wang, Qizhu Wu, Weihong Kuang, Xiaoqi Huang, Yong He, and Qiyong Gong

Background: Neuroimaging studies have shown that major depressive disorder (MDD) is accompanied by structural and functional abnormalities in specific brain regions and connections; yet, little is known about alterations of the topological organization of whole-brain networks in MDD patients.

Methods: Thirty drug-naive, first-episode MDD patients and 63 healthy control subjects underwent a resting-state functional magnetic resonance imaging scan. The whole-brain functional networks were constructed by thresholding partial correlation matrices of 90 brain regions, and their topological properties (e.g., small-world, efficiency, and nodal centrality) were analyzed using graph theory-based approaches. Nonparametric permutation tests were further used for group comparisons of topological metrics.

Results: Both the MDD and control groups showed small-world architecture in brain functional networks, suggesting a balance between functional segregation and integration. However, compared with control subjects, the MDD patients showed altered quantitative values in the global properties, characterized by lower path length and higher global efficiency, implying a shift toward randomization in their brain networks. The MDD patients exhibited increased nodal centralities, predominately in the caudate nucleus and default-mode regions, including the hippocampus, inferior parietal, medial frontal, and parietal regions, and reduced nodal centralities in the occipital, frontal (orbital part), and temporal regions. The altered nodal centralities in the left hippocampus and the left caudate nucleus were correlated with disease duration and severity.

Conclusions: These results suggest that depressive disorder is associated with disruptions in the topological organization of functional brain networks and that this disruption may contribute to disturbances in mood and cognition in MDD patients.

Key Words: Connectome, default-mode, depression, fMRI, graph theory, small-world

Major depressive disorder (MDD) is a psychiatric disease characterized by persistent, pervasive feelings of sadness, guilt, and worthlessness, which results in a greater chance of suicide (1). Major depressive disorder is the most common unipolar affective disorder, with a yearly increase in morbidity and a high risk of mortality. Despite advances in the development of treatment strategies, up to 60% of depression patients suffer at least one recurrence, which causes increasing social and economic burdens (2).

Functional neuroimaging studies have documented that MDD is related to widespread local abnormalities in many brain regions, such as the hippocampus (3), parahippocampal gyrus (4), posterior cingulate gyrus (5), orbitofrontal cortex (4,6), prefrontal cortex (7,8), caudate nucleus (9,10), and occipital regions (4). Moreover, changes in functional connectivity have been found between specific region pairs in MDD, such as decreased orbitofrontal cortex-precuneus connectivity (7), pregenual anterior cingulate cortex-dorsomedial thalamus connectivity (11), and bilateral amygdala connectivity (12) and increased subgenual cingulate-thalamic connectivity (13). Despite the increasing knowledge of MDD, however, very little is known regarding whether MDD disrupts the global topological organization of whole-brain networks.

Recent research has suggested that graph theoretical analysis provides a powerful framework for characterizing topological properties of brain networks (for reviews, see [14–19]). For instance, the normal brain is functionally organized in a small-world fashion (characterized by a high local specialization and a high global integration between brain regions) (20–24). Moreover, such an organization pattern is disrupted in various brain diseases, such as Alzheimer's disease (25–28) and schizophrenia (29–33). To our knowledge, there is only one electroencephalogram study showing the loss of small-world characteristics in the sleep functional brain networks in MDD, suggesting a disruption of topological organization caused by this disease (34). In the current study, we utilized resting-state functional magnetic resonance imaging (R-fMRI) to investigate the topological organization of intrinsic brain networks in patients with MDD.

Resting-state functional magnetic resonance imaging is a noninvasive imaging technique to measure spontaneous brain activity as low-frequency fluctuations in blood oxygen level–dependent signals (35). This technique has been extensively used to reveal the intrinsic typical and atypical functional architecture of the brain (16,36,37). More recently, several groups have applied R-fMRI to investigate MDD-related changes in spontaneous brain activity (11,13,38). These studies mainly focused on functional connectivity, either within a specific brain system or between different systems. The topological organization of whole-brain functional networks in MDD remains poorly understood.

Here, we hypothesize that MDD disrupts the topological organization of intrinsic functional brain networks. To test our hypothesis, we collected R-fMRI data from 30 drug-naive, first-episode MDD patients and 63 healthy control subjects and analyzed their intrinsic brain connectivity networks using graph theoretical approaches. Between-group differences and relationships with clinical variables were investigated.

From the Huaxi Magnetic Resonance Research Center (JZ, QW, XH, QG), Department of Radiology, Center for Medical Imaging, West China Hospital of Sichuan University, Chengdu; State Key Laboratory of Cognitive Neuroscience and Learning (JW, YH), Beijing Normal University, Beijing; and Department of Psychiatry (WK), State Key Laboratory of Biotherapy, West China Hospital of Sichuan University, Chengdu, China.

Authors JZ and JW contributed equally to this work.

Address correspondence to Yong He, Ph.D., Beijing Normal University, State Key Laboratory of Cognitive Neuroscience and Learning, No 19 Xinjiekouwai Street, Haidian District, Beijing, China 100875; E-mail: yong.he@bnu.edu.cn.

Received Feb 5, 2011; revised May 5, 2011; accepted May 23, 2011.

0006-3223/$36.00
doi:10.1016/j.biopsych.2011.05.018

Table 1. Demographics and Clinical Characteristics of the Subjects

	NC ($n = 63$)	MDD ($n = 30$)	p Value
Age (years)	16–81 (35.1 ± 15.9)	18–60 (36.1 ± 12.3)	.765[a]
Gender (male/female)	30/33	8/22	.055[b]
Handedness (R/L)	63/0	30/0	—
Course of Disease (weeks)	NA	2–60 (16.0 ± 14.1)	—
HAMD	NA	18–34 (24.3 ± 5.0)	—
Onset Age (years)	NA	18–59 (35.8 ± 12.2)	—

Data are presented as the range of minimum–maximum (mean ± SD).
HAMD, Hamilton Depression Rating Scale; L, left; MDD, major depressive disorder; NA, nonapplicable; NC, normal control subjects; R, right.
[a]The p value was obtained by two-sample two-tailed t test.
[b]The p value was obtained by two-tailed Pearson chi-square test.

Methods and Materials

Subjects

A total of 95 subjects were recruited, including 31 first-episode drug-naive MDD patients and 64 age- and sex-matched healthy control subjects (Table 1). The age of MDD patients ranged from 18 to 60 years and the age of control subjects ranged from 16 to 81 years. The age of onset of MDD ranged from 18 to 59 years. The data of two subjects (one patient and one control subject) were removed because of excessive head motion (see Data Preprocessing). All patients reported herein were part of a large cohort study of major depression in the Chinese population of Han nationality in the Mental Health Center of West China Hospital. Patients were recruited consecutively from the psychiatric outpatient or inpatient department of the local hospital, and the diagnosis of first-episode depression was made according to the Structured Clinical Interview of the DSM-IV (39). All control subjects were carefully screened for a current or lifetime diagnosis of any Axis I or II disorder using the Structured Clinical Interview of the DSM-IV Non-Patient Edition and Structured Clinical Interview for DSM-IV Axis II Personality Disorders. Neurological or organic disorders were determined according to personal histories and complete physical examinations. The severity of depression was rated using the 17-item Hamilton Rating Scale for Depression (HAMD) (40) and the Clinical Global Impression of Severity scale (41). To be eligible for the study, each patient was re-examined by a psychiatry specialist after an initial outpatient assessment. Inclusion criteria were that all patients were 1) drug-naive and were having their first episode of depression; 2) currently experiencing an episode of depression with HAMD total score ≥ 18 and a Clinical Global Impression of Severity scale score ≥ 4 on the day of the magnetic resonance imaging (MRI) examination; and 3) a duration of depression > 2 weeks but ≤ 60 weeks. Exclusion criteria included the presence of 1) other Axis I psychiatric disorders and symptoms; 2) a history of organic brain disorder, neurological disorders, or cardiovascular diseases; 3) pregnancy or any physical illness as assessed by personal history and laboratory analysis; and 4) the inability to undergo an MRI. No patients were treated with any antipsychotic medicine. All participants were determined to have no abnormalities on conventional MRI by two experienced radiologists. This study was approved by the local ethical committee, and written informed consent was obtained from all subjects.

Image Acquisition

All subjects underwent a resting-state functional MRI scan using a 3T magnetic resonance system (GE EXCITE, Milwaukee, Wisconsin) with an 8-channel phased array head coil. During the scan, subjects were instructed to relax with their eyes closed but not to fall asleep. The scan lasted for 400 seconds. For the details of scanning parameters, see Supplement 1.

Data Preprocessing

Image preprocessing was carried out using the SPM5 package (http://www.fil.ion.ucl.ac.uk/spm; Wellcome Trust Centre for Neuroimaging, University College London, United Kingdom). First, the images were corrected for intravolume acquisition time differences between slices using the sinc interpolation and were corrected for the intervolume geometric displacement because of head movement using a six-parameter (rigid-body) spatial transformation. Data of one control subject and one patient were discarded because their heads moved more than 3 mm of translation or 3 degrees of rotation in any direction. After these corrections, the images were spatially normalized to the standard space of the Montreal Neurological Institute using an optimum 12-parameter affine transformation and nonlinear deformations and resampled to 3-mm cubic voxels. Finally, the resulting data were further temporally bandpass filtered (.01–.1 Hz) to reduce the effects of low-frequency drift and high-frequency physiological noises.

Network Construction

Node Definition. A network is composed of nodes and edges between nodes. Herein, nodes represent brain regions and edges represent the statistical interdependence in blood oxygen level–dependent signals between different regions. To define the brain nodes, a prior atlas of Automated Anatomical Labeling (42) was employed to divide the whole brain into 90 (45 for each hemisphere) cortical and subcortical regions of interest, with each representing a node of the network (Table S1 in Supplement 1).

Edge Definition. To define the network edges, we calculated the partial correlation coefficients between the regional mean time series of all possible pairs of brain regions. The partial correlation coefficient between any two regions represents their conditional dependences by excluding the effects of the other 88 regions defined in the Automated Anatomical Labeling atlas. This metric has been used in previous brain network studies (22,25,33,43–45). Before the correlation analysis, the representative mean time series of each region was acquired by averaging the time series of all voxels within that region, followed by a correction of head motion effects by regressing out the head motion profiles estimated in the image realignment from the mean time course. The residuals of the regression analyses were used to compute the partial correlation in this study, resulting in a 90×90 partial correlation matrix for each subject (Figure S1 in Supplement 1). Finally, individual partial correlation matrices were converted into binarized matrices (i.e., adjacency matrices) $A_{ij}=[a_{ij}]$ according to a predefined threshold (see below for the threshold selection), where the entry a_{ij} was 1 if the absolute value of the partial correlation between regions i and j was larger than the threshold and was 0 otherwise.

Network Analysis

Threshold Selection. We applied a sparsity threshold S to all correlation matrices. S was defined as the ratio of the number of existing edges divided by the maximum possible number of edges in a network. This approach normalized all resultant networks to have the same number of nodes and edges by applying a subject-specific correlation coefficient threshold and minimized the effects of possible discrepancies in the overall correlation strength between groups, thereby enabling us to explore the between-group differences in relative network organization (46,47). Instead of selecting a single threshold, we thresholded each correlation matrix repeatedly over a wide range of sparsity levels according to the

following criteria: 1) the average degree (the degree of a node is the number of connections linked to the node) over all nodes of each thresholded network was larger than $2 \times \log(N)$ with $N = 90$ here, denoting the number of nodes; and 2) the small-worldness scalar σ (see below for definition) of the thresholded networks was larger than 1.1 for all participants (Figure S2 in Supplement 1). The generated threshold range of $.10 < S < .34$ determined by this procedure guaranteed that the thresholded networks were estimable for small-worldness (48) and had sparse properties with as few spurious edges as possible (25,46,49). The largest component sizes of individual networks were from 88 to 90 over the sparsity range (Figure S3 in Supplement 1). The subsequent network analyses were repeatedly performed in the accurately defined small-world regime of $.10 < S < .34$ with an interval of .01.

Network Metrics. For brain networks at each sparsity threshold, we calculated both global and regional network measures. The global measures included 1) small-world parameters (48) involving clustering coefficient $^{C}_{p}$, characteristic path length $^{L}_{p}$, normalized clustering coefficient γ, normalized characteristic path length λ, and small-worldness σ; and 2) network efficiency (50) involving local efficiency $^{E}_{loc}$ and global efficiency $^{E}_{glob}$. The regional measures included three nodal centrality metrics: the degreeκ, efficiency *e*, and betweenness *b* (46,51) (for a recent review on uses and interpretations of these network measures, see [18] and Supplement 1). Furthermore, we calculated the area under the curve (AUC) for each network metric (for the illustration of AUC, see Figure S4 in Supplement 1), which provides a summarized scalar for topological characterization of brain networks independent of single threshold selection. The integrated AUC metric has been used in previous brain network studies and is sensitive at detecting topological alterations of brain disorders (46,47,52).

To further localize specific pairs of brain regions in which functional connectivity was altered in patients, we used a network-based statistic (NBS) approach (53). Briefly, we identified region pairs showing between-group differences in functional connectivity and utilized the NBS method to localize those connected networks showing significant changes in the MDD patients (Supplement 1).

Statistical Analysis

Differences in Network Metrics. To determine whether there existed significant group differences in the network properties, nonparametric permutation tests (54) were performed on the AUC of each network metric (small-world, network efficiency and regional centrality measures). Briefly, we first calculated the between-group difference in the mean value of each network metric. To test the null hypothesis that the observed group differences could occur by chance, for each network metric we then randomly reallocated all the values into two groups and recomputed the mean differences between the two randomized groups. This randomization procedure was repeated 10,000 times, and the 95th percentile points of each distribution were used as the critical values for a one-tailed test of the null hypothesis with a probability of type I error of .05. Of note, before the permutation tests, multiple linear regression analyses were applied to remove the confounding effects of age and gender for each network metric (independent variable: the AUC of each network metric; dependent variables: age and gender). Likewise, permutation tests were used to determine the significance levels of altered connectivity networks in the NBS analysis (Supplement 1).

Relationships Between Network Measures and Clinical Variables. Once significant between-group differences were observed in any network metrics, we further assessed the relationships between these metrics and the HAMD score and the course of disease in the MDD group, performed by multiple linear regression analyses with age and gender as unconcerned confounding factors (independent variables: network metrics showing between-group differences; dependent variables: clinical characteristics of the HAMD score or course of disease).

Results

Efficient Small-World Functional Brain Networks

The topological properties of brain networks depend on the choices of thresholds. In the current study, we determined a data-specific small-world regime at a sparsity range of $.10 < S < .34$. Partial correlation thresholds ranged from .42 to .47 (mean $\pm$ SD = .44 $\pm$ .01) at $S = .10$ and from .25 to .28 (mean $\pm$ SD = .26 $\pm$ .01) at $S = .34$ across all subjects. In the precisely defined threshold range, functional brain networks of both the MDD and control groups had higher clustering coefficients (i.e., $\gamma > 1$) but almost identical characteristic path lengths (i.e., $\lambda \approx 1$), compared with comparable random networks (Figure 1A and Figure S5A in Supplement 1), which are typical features of small-worldness. Moreover, using more biologically relevant network efficiency measurements, all brain networks also demonstrated an economic small-world topology of approximately equivalent parallel information processing of global efficiency but a higher fault tolerance of local efficiency compared with matched random networks (Figure 1B and Figure S5B in Supplement 1). These results are compatible with previous studies of small-world brain networks (for reviews, see [15,17,55]).

MDD-Related Alterations in Small-World Properties

Despite common small-world architecture, statistical analyses revealed significant differences in both small-world parameters and network efficiency between MDD patients and control subjects (Figure 2). The MDD group showed significantly lower values in both the characteristic path length $^{L}_{p}$ ($p = .020$) and normalized characteristic path length λ ($p = .020$) compared with normal control subjects. No significant ($p > .05$) differences were found in local clustering of $^{C}_{p}$ and γ. As to network efficiency, the comparisons revealed a significantly increased global efficiency $^{E}_{glob}$ ($p = .020$) but unchanged local efficiency $^{E}_{loc}$ ($p > .05$) in the functional brain networks of MDD patients as compared with normal control subjects.

MDD-Related Alterations in Regional Nodal Characteristics

We identified the brain regions showing significant between-group differences in at least one nodal metric ($p < .05$, uncorrected). Compared with normal control subjects, MDD patients showed increased nodal centralities in many brain regions, including the bilateral hippocampus, the bilateral caudate nucleus, the left inferior parietal lobe, the left precuneus, the left parahippocampal gyrus, the left postcentral gyrus, the left putamen, the right supramarginal gyrus, and the right superior frontal gyrus (medial orbital) (Figure 3A, Table 2). Most of these regions were the components of the default-mode network (DMN) (56–58). Decreased nodal centralities in MDD patients were predominantly located in several regions of the occipital (the bilateral lingual gyrus, the right calcarine fissure and surrounding cortex, and the left cuneus), frontal (the orbital part of left superior and middle frontal gyrus and the right middle frontal gyrus), and temporal (the right middle temporal gyrus) lobes (Figure 3A, Table 2).

MDD-Related Alterations in Functional Connectivity

We utilized the NBS method to identify a single connected network with 12 nodes and 12 connections, which was significantly

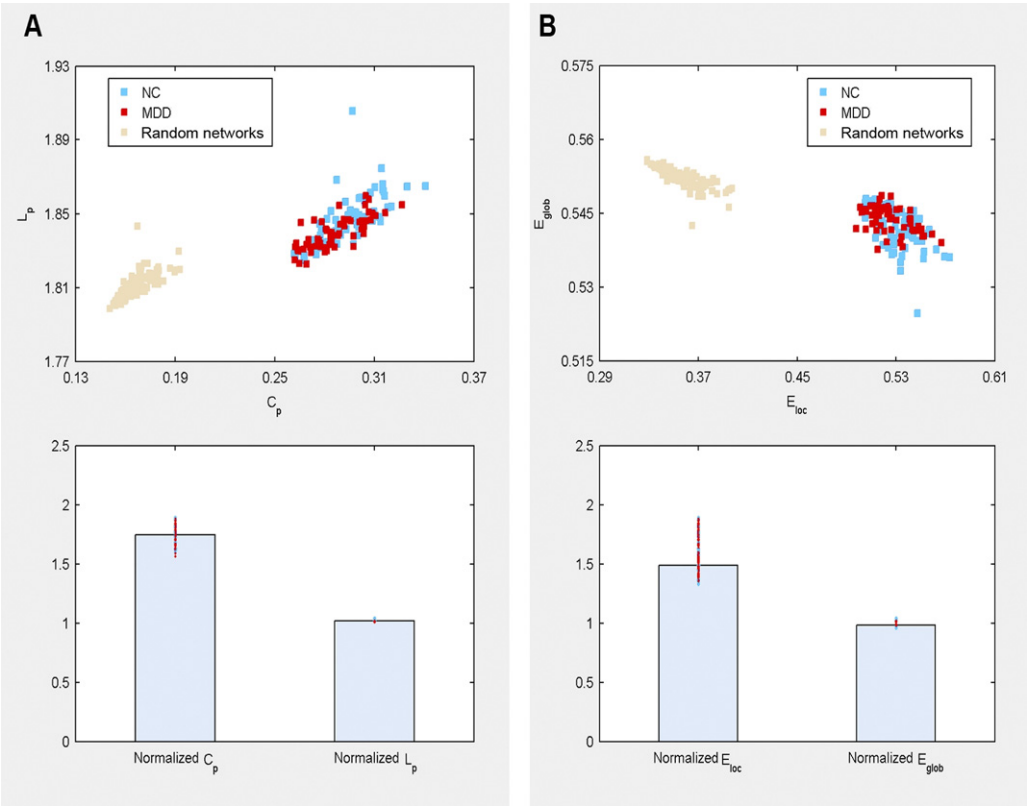

Figure 1. The small-world parameters and network efficiency of functional brain networks. **(A)** Functional brain networks of both MDD patients and NC showed a higher clustering coefficient ($^{C}_{p}$) and approximately equal characteristic path length ($^{L}_{p}$) compared with matched random networks (top panel), resulting in normalized $^{C}_{p}$ (i.e.,γ) > 1 and normalized $^{L}_{p}$ (i.e., λ) ≈ 1 (bottom panel). **(B)** Functional brain networks exhibited higher local network efficiency ($^{E}_{loc}$) but approximately identical global efficiency ($^{E}_{glob}$) of parallel information transmission compared with matched random networks (top panel), resulting in normalized $^{E}_{loc} > 1$ and normalized $^{E}_{glob} \approx 1$ (bottom panel). Thus, both small-world parameters and network efficiency suggest a small-world topology for functional brain networks of all participants. Of note, the results are represented only for functional brain networks constructed at a threshold level of $S = .15$. For the results at other threshold levels, see Figure S5 in Supplement 1. MDD, major depressive disorder; NC, normal control subjects.

altered in the patients ($p = .002$, corrected) (Figure 4, Table S2 in Supplement 1). The nodes included several default-mode regions (e.g., precuneus, lateral temporal, and parietal regions) and the connections were mainly involved in the long-distance connections linking different lobes. Within this network, all connections exhibited increased values in the MDD patients as compared with the control subjects. The mean connectivity value showed marginally significant correlations with the three global network metrics ($^{L}_{p}$: $p = .059$; λ: $p = .056$; $^{E}_{glob}$: $p = .051$) (Figure 4).

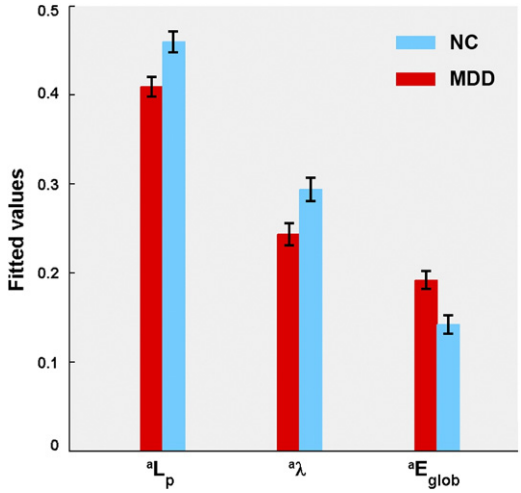

Figure 2. Differences in topological properties of functional brain networks between MDD patients and NC. [a]Significant differences were found in characteristic path length $^{L}_{p}$ ($p = .020$), normalized characteristic path length λ ($p = .020$), and global efficiency $^{E}_{glob}$ ($p = .020$) between MDD patients and NC. Error bars denote standard deviations. MDD, major depressive disorder; NC, normal control subjects.

Relationships Between Network Measures and Clinical Variables

There were no significant ($p > .05$) correlations between global network metrics ($^{C}_{p}$, $^{L}_{p}$, γ, λ, $^{E}_{loc}$, and $^{E}_{glob}$) and clinical variables (HAMD scores or the duration of illness). There were also no significant ($p > .05$) correlations between mean connectivity values within the NBS-based network and clinical characteristics. The left hippocampus was negatively ($p < .05$) correlated with both HAMD scores and the duration of illness. The left caudate nucleus was positively ($p < .05$) correlated with HAMD scores in at least one nodal measure (Figure 3B). The left precuneus showed marginally significant ($.05 < p < .10$) correlation with HAMD scores (Figure 3B).

Discussion

The present study examined the topological organization of functional brain networks in MDD patients. The results reveal that MDD had decreased path length and increased global efficiency, implying a disturbance of the normal global integration of whole-

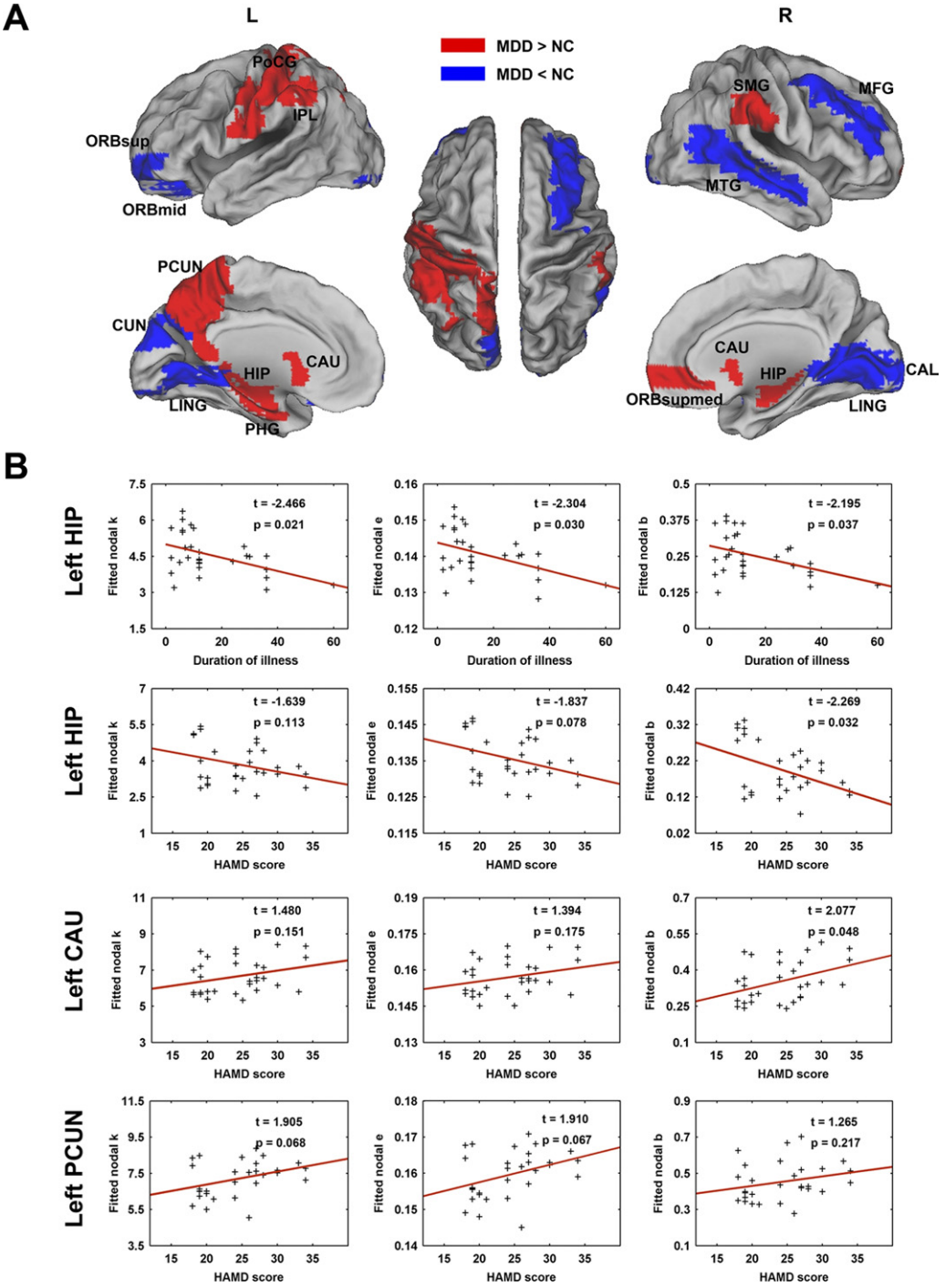

Figure 3. Brain regions showing abnormal nodal centralities in brain functional networks and their relationships with clinical variables in MDD patients. **(A)** Regions with abnormal nodal centralities in MDD patients were rendered on the surface of the Population-Average, Landmark- and Surface-based atlas based on structural MRI volumes from 12 normal subjects (PALS-B12) in Computerized Anatomical Reconstruction and Editing Toolkit (CARET; http://brainvis.wustl.edu). See Table 2 for the detailed information. **(B)** Scatter plots of nodal metrics against disease duration and HAMD scores. A subcortical region (the lenticular nucleus, putamen) showed group differences in nodal centrality but is not shown here. CAL, calcarine fissure and surrounding cortex; CAU, caudate nucleus; CUN, cuneus; HAMD, Hamilton Depression Rating Scale; HIP, hippocampus; IPL, inferior parietal, but supramarginal and angular gyri; L, left hemisphere; LING, lingual gyrus; MDD, major depressive disorder; MFG, middle frontal gyrus; MTG, middle temporal gyrus; NC, normal control subjects; ORBmid, middle frontal gyrus, orbital part; ORBsup, superior frontal gyrus, orbital part; ORBsupmed, superior frontal gyrus, medial orbital; PCUN, precuneus; PHG, parahippocampal gyrus; PoCG, postcentral gyrus; R, right hemisphere; SMG, supramarginal gyrus.

brain networks. Moreover, many local brain regions were profoundly affected by MDD: both caudate nucleus and default-mode regions showed increased nodal centralities, while several regions in the occipital, frontal, and temporal lobes showed decreased centralities. These results provide insights into our understanding of altered topological organization in functional brain networks of MDD.

Table 2. Regions Showing Abnormal Nodal Centralities in MDD Patients as Compared with Control Subjects

Brain Regions	*p* Values		
	Nodal Degree	Nodal Efficiency	Nodal Betweenness
MDD > Control Subjects			
Right hippocampus	**.008**	**.010**	**.048**
Right caudate nucleus	**.021**	**.033**	**.047**
Left hippocampus	**.025**	**.012**	.172
Left caudate nucleus	**.027**	**.033**	**.036**
Left inferior parietal, but supramarginal and angular gyri	**.031**	**.025**	**.009**
Left putamen	**.036**	**.034**	.088
Left precuneus	**.036**	**.035**	**.015**
Right supramarginal gyrus	.060	**.027**	.064
Left parahippocampal gyrus	.067	**.040**	.159
Right superior frontal gyrus, medial orbital	.076	**.044**	.220
Left postcentral gyrus	.071	**.049**	**.045**
MDD < Control Subjects			
Left lingual gyrus	**.009**	**.015**	**.047**
Right calcarine fissure and surrounding cortex	**.012**	**.016**	.052
Left middle frontal gyrus, orbital part	**.023**	**.048**	**.005**
Left cuneus	**.024**	**.025**	**.020**
Right middle frontal gyrus	**.034**	**.038**	.071
Right lingual gyrus	**.040**	**.037**	.157
Left superior frontal gyrus, orbital part	**.041**	.060	.165
Right middle temporal gyrus	**.041**	**.026**	.076

Regions were considered abnormal in MDD patients if they exhibited significant between-group differences ($p < .05$, uncorrected) in at least one of the three nodal centralities (shown in bold font).

MDD, major depressive disorder.

The human brain is a complex, interconnected system and has various important topological attributes, such as small-worldness, high efficiency at a low wiring cost, and highly connected hubs (15–17,55,59). In a small-world network, nodes are locally clustered in favor of modular information processing on the one hand and are efficient in overall routing with the addition of few long-range connections or shortcuts on the other hand (48). More recently, Latora and Marchiori (50) expanded the theory of small-worldness in terms of the two measures of efficiency and cost. Networks that are cheap to build but still efficient in propagating information are said to be economic small-world networks. Small-worldness is an attractive model to characterize brain networks because the combination of high local clustering and short path length supports the two fundamental organizational principles in the brain: functional segregation and functional integration. Here, using both the conventional small-world model and novel efficiency measures, we found that both MDD patients and control subjects showed efficient small-world topology in whole-brain functional networks.

Despite the common small-world topology, there were significant group differences in small-world metrics and network efficiency. The MDD patients showed a decreased path length in their brain networks as compared with control subjects, whereas there were no significant differences in local clustering. Likewise, network efficiency analysis revealed abnormal small-world organization in the MDD group, as characterized by increased global efficiency. The changes in these global network metrics could be attributable to increased long-distance functional connections in patients, involving a specific connected network mainly comprising default-mode regions (Figure 4, Table S2 in Supplement 1). Notably, a previous electroencephalogram study reported that depressed patients showed a significantly lower path length in the theta and delta frequency bands but no significant changes in clustering coefficient (34), providing further support for our findings. Given that the small-world model reflects an optimal balance between local specialization and global integration, these results thus indicate a disturbance of the normal balance in functional brain networks of MDD patients. Specifically, the findings of increased global integration and maintained local specialization in the patients suggest that functional brain networks in MDD are closer to a randomized configuration. This randomization process has been observed in brain functional networks in other neuropsychiatry diseases, such as Alzheimer's disease (27) and schizophrenia (30). Random networks have less modularized information processing or fault tolerance compared with small-world networks (50). Therefore, our findings of loss of small-world characteristics in MDD reflect a less optimal topological organization in brain networks, thus providing further evidence that MDD is a disorder with disrupted neuronal network organization and deficient cognitive and mood processing.

The MDD-related increases in nodal centralities were mainly found in the hippocampus, parahippocampal gyrus, medial frontal and parietal regions, and inferior parietal lobe, most of which are components of the DMN (56–58). Several DMN regions have shown depression-related increases in regional cerebral blood flow to the hippocampus (3) and cerebral metabolism in the parahippocampal gyrus (2,5), precuneus (2), and posterior cingulate cortex (5). Moreover, DMN-related increases of functional connectivity have also been observed in depressed patients, such as between the subgenual cingulate and thalamus (13) and within the DMN regions (38). In this study, we also found MDD-related increases in nodal centralities in the caudate nucleus, a key brain structure involved in the regulation of cognition and mood (60). Major depressive disorder patients exhibited reduced gray matter volume in the caudate nucleus (61–63) and abnormal brain activities during specific tasks or in a resting state (9,64,65). Particularly, a recent fMRI study showed that MDD patients had increased neuronal responses in the caudate nucleus to emotional faces in a facial expression matching

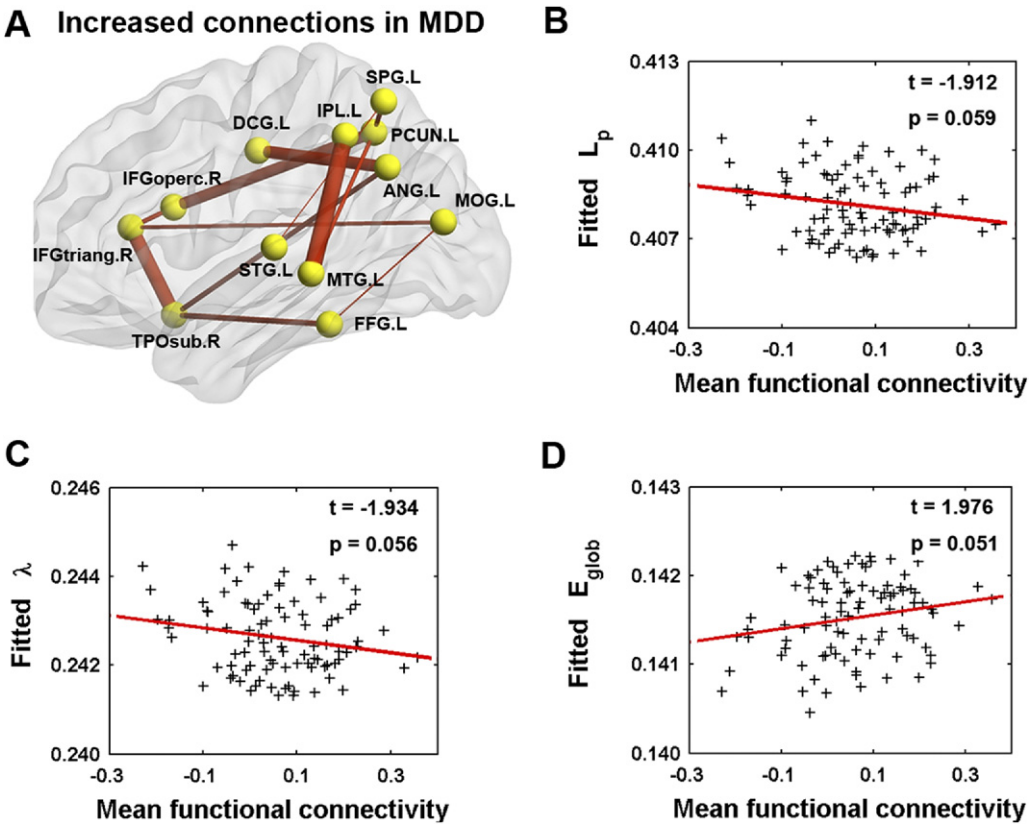

Figure 4. The connected network showing increased functional connections in MDD patients and its relationships with the global network metrics. **(A)** The region pairs showing increased functional connections in MDD patients. These connections formed a single connected network with 12 nodes and 12 connections, which was significantly ($p = .002$, corrected) abnormal in the patients. Of note, 9 of 12 connections are long-distance connections that link different lobes. The nodes and connections were mapped onto the cortical surfaces using in-house BrainNet viewer software. For the details, see Table S2 in Supplement 1. **(B-D)** Scatter plots of mean functional connectivity of this connected network against global network metrics. There were marginally significant correlations with the three metrics ($^{L}_{p}$: $p = .059$; λ: $p = .056$; $^{E}_{glob}$: $p = .051$). ANG, angular gyrus; DCG, median cingulate and paracingulate gyri; E_{glob}, global efficiency; FFG, fusiform gyrus; IFGoperc, inferior frontal gyrus (opercular part); IFGtriang, inferior frontal gyrus (triangular part); IPL, inferior parietal lobe; L, left hemisphere; L_p, characteristic path length; MDD, major depressive disorder; MOG, middle occipital gyrus; MTG, middle temporal gyrus; λ, normalized characteristic path length; PCUN, precuneus; R, right hemisphere; SPG, superior parietal gyrus; STG, superior temporal gyrus; TPOsub, superior temporal gyrus (temporal pole).

task (10). Thus, our findings are compatible with these previous studies. Increased nodal centralities of these regions suggest their strengthened roles of coordinating whole-brain networks, presumably in response to the pathological disorder of MDD.

Specifically, we found that nodal centralities of the left hippocampus were negatively related to the duration of the disease, indicating the longer the illness, the lower the nodal centralities of the left hippocampus. Hippocampal volume is believed to decrease in depression patients (66–68), and this shrinkage is positively correlated with depressive duration (69–71). In our sample, the left hippocampus was negatively related to depression severity (HAMD scores). de Asis *et al.* (72) reported that hippocampal hypoactivation might constitute neural substrates of geriatric depression. The depressive state can be predicted by hippocampus-related morphological changes (70) or resting-state functional connectivity (73). Thus, our finding in the hippocampus is consistent with previous studies and suggests its role in predicting the depressive state. Of note, recent research on first-episode, drug-naive MDD patients has indicated that hippocampal volume is positively correlated with symptom severity (74), whereas it is negatively correlated with disease duration in MDD (75,76). These results suggest the opposite mechanism of depressive symptom severity and duration on the volume of the hippocampus. Given the increased nodal centrality of the hippocampus in MDD patients, we speculate that disease severity and duration also have competitive effects on the intrinsic activity of the left hippocampus.

The MDD-related decreases in nodal centralities were mainly observed in occipital cortex regions, including the calcarine fissure, cuneus, and lingual gyrus. Depression has been associated with both structural and functional abnormalities in occipital regions, such as decreased gray matter volume in the cuneus (77) and decreased cerebral blood flow in the lingual gyrus (78). Moreover, evidence from first-episode, treatment-naive MDD patients has shown decreased white matter integrity related to occipital regions (79). Our findings are consistent with these. In addition, fewer nodal centralities were found in the middle frontal gyrus (orbital part), which is also compatible with a previous study showing frontal white matter lesions (79).

Several issues need to be further addressed. First, the head motions of subjects might have confounded our results. Further analyses revealed no significant group differences in the head motion profiles and no significant correlations between head motions and the network metrics. Second, in the current study, functional brain networks were constructed at a regional level by parcellating the whole brain into 90 regions based on a previously published atlas. Brain networks derived using different parcellation schemes

or at different spatial scales exhibit distinct topological architectures (52,80–83). Further studies are needed to determine which brain parcellation strategy or spatial scale is most appropriate for the characterization of network topology in MDD. Third, the nodal centrality results were not corrected by multiple comparisons, meaning this should be considered an exploratory analysis. To increase statistical power, future studies need to be conducted using a large sample of MDD patients or by selecting a limited number of regions of interest. Fourth, the recruited MDD patients were heterogeneous in terms of symptom clusters. A previous fMRI study (84) suggests that different MDD symptom dimensions could have distinct neuronal mechanisms. In the future, it would be interesting to investigate whether patients with different MDD symptoms show distinct topological organizations in their brain networks. Finally, functional brain networks constructed from R-fMRI data are largely constrained by anatomical pathways (85,86). Accordingly, a combined analysis of multimodal imaging data will produce more fruitful information on the interaction between brain function and structure under pathological conditions.

This study was supported by the National Natural Science Foundation of China (Grant Nos. 81030027, 81030028, and 30870667) and the National Basic Research Program of China (973 Program No: 2007CB512305). Drs. Yong He and Qiyong Gong contributed equally to playing the role of corresponding author, and in particular, Dr Qiyong Gong acknowledges the support from his China Medical Board (CMB) Distinguished Professorship Award administered by the Institute of International Education, USA.

The authors reported no biomedical financial interests or potential conflicts of interest.

Supplementary material cited in this article is available online.

1. Jia Z, Huang X, Wu Q, Zhang T, Lui S, Zhang J, *et al.* (2010): High-field magnetic resonance imaging of suicidality in patients with major depressive disorder. *Am J Psychiatry* 167:1381–1390.
2. Smith GS, Kramer E, Hermann C, Ma Y, Dhawan V, Chaly T, Eidelberg D (2009): Serotonin modulation of cerebral glucose metabolism in depressed older adults. *Biol Psychiatry* 66:259–266.
3. Lui S, Parkes LM, Huang X, Zou K, Chan RC, Yang H, *et al.* (2009): Depressive disorders: Focally altered cerebral perfusion measured with arterial spin-labeling MR imaging. *Radiology* 251:476–484.
4. Gilbert AM, Prasad K, Goradia D, Nutche J, Keshavan M, Frank E (2010): Grey matter volume reductions in the emotion network of patients with depression and coronary artery disease. *Psychiatry Res* 181:9–14.
5. Mah L, Zarate CA, Singh J, Duan YF, Luckenbaugh DA, Manji HK, Drevets WC (2007): Regional cerebral glucose metabolic abnormalities in bipolar II depression. *Biol Psychiatry* 61:765–775.
6. Yao Z, Wang L, Lu Q, Liu H, Teng G (2009): Regional homogeneity in depression and its relationship with separate depressive symptom clusters: A resting-state fMRI study. *J Affect Disord* 115:430–438.
7. Frodl T, Scheuerecker J, Albrecht J, Kleemann AM, Müller-Schunk S, Koutsouleris N, *et al.* (2009): Neuronal correlates of emotional processing in patients with major depression. *World J Biol Psychiatry* 10:202–208.
8. Kennedy SH, Konarski JZ, Segal ZV, Lau MA, Bieling PJ, McIntyre RS, Mayberg HS (2007): Differences in brain glucose metabolism between responders to CBT and venlafaxine in a 16-week randomized controlled trial. *Am J Psychiatry* 164:778–788.
9. Brody AL, Saxena S, Stoessel P, Gillies LA, Fairbanks LA, Alborzian S, *et al.* (2001): Regional brain metabolic changes in patients with major depression treated with either paroxetine or interpersonal therapy: Preliminary findings. *Arch Gen Psychiatry* 58:631–640.
10. Norbury R, Selvaraj S, Taylor MJ, Harmer C, Cowen PJ (2010): Increased neural response to fear in patients recovered from depression: A 3T functional magnetic resonance imaging study. *Psychol Med* 40:425–432.
11. Anand A, Li Y, Wang Y, Lowe MJ, Dzemidzic M (2009): Resting state corticolimbic connectivity abnormalities in unmedicated bipolar disorder and unipolar depression. *Psychiatry Res* 171:189–198.
12. Veer IM, Beckmann CF, Baerends E, van Tol MJ, Ferrarini L, Milles JR, *et al.* (2009): Reduced functional connectivity in major depression: A whole brain study of multiple resting-state networks. *Neuroimage* 47(suppl 1):S70.
13. Greicius MD, Flores BH, Menon V, Glover GH, Solvason HB, Kenna H, *et al.* (2007): Resting-state functional connectivity in major depression: Abnormally increased contributions from subgenual cingulate cortex and thalamus. *Biol Psychiatry* 62:429–437.
14. Bassett DS, Bullmore ET (2009): Human brain networks in health and disease. *Curr Opin Neurol* 22:340–347.
15. Bullmore E, Sporns O (2009): Complex brain networks: Graph theoretical analysis of structural and functional systems. *Nat Rev Neurosci* 10:186–198.
16. Wang J, Zuo X, He Y (2010): Graph-based network analysis of resting-state functional MRI. *Front Syst Neurosci* 4:16.
17. He Y, Evans A (2010): Graph theoretical modeling of brain connectivity. *Curr Opin Neurol* 23:341–350.
18. Rubinov M, Sporns O (2010): Complex network measures of brain connectivity: Uses and interpretations. *Neuroimage* 52:1059–1069.
19. Stam CJ (2010): Characterization of anatomical and functional connectivity in the brain: A complex networks perspective. *Int J Psychophysiol* 77:186–194.
20. Achard S, Salvador R, Whitcher B, Suckling J, Bullmore E (2006): A resilient, low-frequency, small-world human brain functional network with highly connected association cortical hubs. *J Neurosci* 26:63–72.
21. He Y, Chen ZJ, Evans AC (2007): Small-world anatomical networks in the human brain revealed by cortical thickness from MRI. *Cereb Cortex* 17: 2407–2419.
22. Salvador R, Suckling J, Coleman MR, Pickard JD, Menon D, Bullmore E (2005): Neurophysiological architecture of functional magnetic resonance images of human brain. *Cereb Cortex* 15:1332–1342.
23. Hagmann P, Kurant M, Gigandet X, Thiran P, Wedeen VJ, Meuli R, Thiran JP (2007): Mapping human whole-brain structural networks with diffusion MRI. *PLoS ONE* 2:e597.
24. Stam CJ (2004): Functional connectivity patterns of human magnetoencephalographic recordings: A "small-world" network? *Neurosci Lett* 355: 25–28.
25. He Y, Chen Z, Evans A (2008): Structural insights into aberrant topological patterns of large-scale cortical networks in Alzheimer's disease. *J Neurosci* 28:4756–4766.
26. Supekar K, Menon V, Rubin D, Musen M, Greicius MD (2008): Network analysis of intrinsic functional brain connectivity in Alzheimer's disease. *PLoS Comput Biol* 4:e1000100.
27. Stam CJ, de Haan W, Daffertshofer A, Jones BF, Manshanden I, van Cappellen van Walsum AM, *et al.* (2009): Graph theoretical analysis of magnetoencephalographic functional connectivity in Alzheimer's disease. *Brain* 132:213–224.
28. Lo CY, Wang PN, Chou KH, Wang J, He Y, Lin CP (2010): Diffusion tensor tractography reveals abnormal topological organization in structural cortical networks in Alzheimer's disease. *J Neurosci* 30:16876–16885.
29. Yu Q, Sui J, Rachakonda S, He H, Pearlson G, Calhoun VD (2011): Altered small-world brain networks in temporal lobe in patients with schizophrenia performing an auditory oddball task. *Front Syst Neurosci* 5:7.
30. Lynall ME, Bassett DS, Kerwin R, McKenna PJ, Kitzbichler M, Muller U, Bullmore E (2010): Functional connectivity and brain networks in schizophrenia. *J Neurosci* 30:9477–9487.
31. van den Heuvel MP, Mandl RC, Stam CJ, Kahn RS, Hulshoff Pol HE (2010): Aberrant frontal and temporal complex network structure in schizophrenia: A graph theoretical analysis. *J Neurosci* 30:15915–15926.
32. Zalesky A, Fornito A, Seal ML, Cocchi L, Westin CF, Bullmore ET, *et al.* (2011): Disrupted axonal fiber connectivity in schizophrenia. *Biol Psychiatry* 69:80–89.
33. Liu Y, Liang M, Zhou Y, He Y, Hao Y, Song M, *et al.* (2008): Disrupted small-world networks in schizophrenia. *Brain* 131:945–961.
34. Leistedt SJ, Coumans N, Dumont M, Lanquart JP, Stam CJ, Linkowski P (2009): Altered sleep brain functional connectivity in acutely depressed patients. *Hum Brain Mapp* 30:2207–2219.
35. Biswal B, Yetkin FZ, Haughton VM, Hyde JS (1995): Functional connectivity in the motor cortex of resting human brain using echo-planar MRI. *Magn Reson Med* 34:537–541.
36. Fox MD, Raichle ME (2007): Spontaneous fluctuations in brain activity observed with functional magnetic resonance imaging. *Nat Rev Neurosci* 8:700–711.
37. Zhang D, Raichle ME (2010): Disease and the brain's dark energy. *Nat Rev Neurol* 6:15–28.

38. Sheline YI, Price JL, Yan Z, Mintun MA (2010): Resting-state functional MRI in depression unmasks increased connectivity between networks via the dorsal nexus. *Proc Natl Acad Sci U S A* 107:11020–11025.
39. First M, Spitzer R, Gibbon M, Williams J (1997): *Structured Clinical Interview for DSM-IV Axis I Disorders*. Washington, DC: American Psychiatric Publishing.
40. Williams JB (1988): A structured interview guide for the Hamilton Depression Rating Scale. *Arch Gen Psychiatry* 45:742–747.
41. Guy W (1976): ECDEU Assessment Manual for Psychopharmacology. Rockville, MD: National Institute of Mental Health.
42. Tzourio-Mazoyer N, Landeau B, Papathanassiou D, Crivello F, Etard O, Delcroix N, *et al.* (2002): Automated anatomical labeling of activations in SPM using a macroscopic anatomical parcellation of the MNI MRI single-subject brain. *Neuroimage* 15:273–289.
43. Ferrarini L, Veer IM, Baerends E, van Tol MJ, Renken RJ, van der Wee NJ, *et al.* (2009): Hierarchical functional modularity in the resting-state human brain. *Hum Brain Mapp* 30:2220–2231.
44. Liu P, Zhang Y, Zhou G, Yuan K, Qin W, Zhuo L, *et al.* (2009): Partial correlation investigation on the default mode network involved in acupuncture: An fMRI study. *Neurosci Lett* 462:183–187.
45. Nakamura T, Hillary FG, Biswal BB (2009): Resting network plasticity following brain injury. *PLoS ONE* 4:e8220.
46. Achard S, Bullmore E (2007): Efficiency and cost of economical brain functional networks. *PLoS Comput Biol* 3:e17.
47. He Y, Dagher A, Chen Z, Charil A, Zijdenbos A, Worsley K, Evans A (2009): Impaired small-world efficiency in structural cortical networks in multiple sclerosis associated with white matter lesion load. *Brain* 132:3366–3379.
48. Watts DJ, Strogatz SH (1998): Collective dynamics of "small-world" networks. *Nature* 393:440–442.
49. Bassett DS, Bullmore E, Verchinski BA, Mattay VS, Weinberger DR, Meyer-Lindenberg A (2008): Hierarchical organization of human cortical networks in health and schizophrenia. *J Neurosci* 28:9239–9248.
50. Latora V, Marchiori M (2001): Efficient behavior of small-world networks. *Phys Rev Lett* 87:198701.
51. Freeman LC (1977): A set of measures of centrality based on betweenness. *Sociometry* 40:35–41.
52. Wang J, Wang L, Zang Y, Yang H, Tang H, Gong Q, *et al.* (2009): Parcellation-dependent small-world brain functional networks: A resting-state fMRI study. *Hum Brain Mapp* 30:1511–1523.
53. Zalesky A, Fornito A, Bullmore ET (2010): Network-based statistic: Identifying differences in brain networks. *Neuroimage* 53:1197–1207.
54. Bullmore ET, Suckling J, Overmeyer S, Rabe-Hesketh S, Taylor E, Brammer MJ (1999): Global, voxel, and cluster tests, by theory and permutation, for a difference between two groups of structural MR images of the brain. *IEEE Trans Med Imaging* 18:32–42.
55. Bullmore ET, Bassett DS (2011): Brain graphs: Graphical models of the human brain connectome. *Annu Rev Clin Psychol* 7:113–140.
56. Buckner RL, Andrews-Hanna JR, Schacter DL (2008): The brain's default network: Anatomy, function, and relevance to disease. *Ann N Y Acad Sci* 1124:1–38.
57. Greicius MD, Krasnow B, Reiss AL, Menon V (2003): Functional connectivity in the resting brain: A network analysis of the default mode hypothesis. *Proc Natl Acad Sci U S A* 100:253–258.
58. Raichle ME, MacLeod AM, Snyder AZ, Powers WJ, Gusnard DA, Shulman GL (2001): A default mode of brain function. *Proc Natl Acad Sci U S A* 98:676–682.
59. Sporns O (2011): The human connectome: A complex network. *Ann N Y Acad Sci* 1224:109–125.
60. Lehericy S, Gerardin E (2002): Normal functional imaging of the basal ganglia. *Epileptic Disord* 4(suppl 3):S23–S30.
61. Gabbay V, Hess DA, Liu S, Babb JS, Klein RG, Gonen O (2007): Lateralized caudate metabolic abnormalities in adolescent major depressive disorder: A proton MR spectroscopy study. *Am J Psychiatry* 164:1881–1889.
62. Kim MJ, Hamilton JP, Gotlib IH (2008): Reduced caudate gray matter volume in women with major depressive disorder. *Psychiatry Res* 164:114–122.
63. Krishnan KR, McDonald WM, Escalona PR, Doraiswamy PM, Na C, Husain MM, *et al.* (1992): Magnetic resonance imaging of the caudate nuclei in depression. Preliminary observations. *Arch Gen Psychiatry* 49:553–557.
64. Wu QZ, Li DM, Kuang WH, Zhang TJ, Lui S, Huang XQ, *et al.* (2010): Abnormal regional spontaneous neural activity in treatment-refractory depression revealed by resting-state fMRI [published online ahead of print July 27]. *Hum Brain Mapp*. doi:10.1002/hbm.21108.
65. Pizzagalli DA, Holmes AJ, Dillon DG, Goetz EL, Birk JL, Bogdan R, *et al.* (2009): Reduced caudate and nucleus accumbens response to rewards in unmedicated individuals with major depressive disorder. *Am J Psychiatry* 166:702–710.
66. Bremner JD, Narayan M, Anderson ER, Staib LH, Miller HL, Charney DS (2000): Hippocampal volume reduction in major depression. *Am J Psychiatry* 157:115–117.
67. Czéh B, Lucassen PJ (2007): What causes the hippocampal volume decrease in depression? Are neurogenesis, glial changes and apoptosis implicated? *Eur Arch Psychiatry Clin Neurosci* 257:250–260.
68. Gonul AS, Kitis O, Eker MC, Eker OD, Ozan E, Coburn K (2011): Association of the brain-derived neurotrophic factor Val66Met polymorphism with hippocampus volumes in drug-free depressed patients. *World J Biol Psychiatry* 12:110–118.
69. Campbell S, Macqueen G (2004): The role of the hippocampus in the pathophysiology of major depression. *J Psychiatry Neurosci* 29:417–426.
70. MacQueen GM (2009): Magnetic resonance imaging and prediction of outcome in patients with major depressive disorder. *J Psychiatry Neurosci* 34:343–349.
71. Sheline YI, Sanghavi M, Mintun MA, Gado MH (1999): Depression duration but not age predicts hippocampal volume loss in medically healthy women with recurrent major depression. *J Neurosci* 19:5034–5043.
72. de Asis JM, Stern E, Alexopoulos GS, Pan H, Van Gorp W, Blumberg H, *et al.* (2001): Hippocampal and anterior cingulate activation deficits in patients with geriatric depression. *Am J Psychiatry* 158:1321–1323.
73. Craddock RC, Holtzheimer PE 3rd, Hu XP, Mayberg HS (2009): Disease state prediction from resting state functional connectivity. *Magn Reson Med* 62:1619–1628.
74. Cheng YQ, Xu J, Chai P, Li HJ, Luo CR, Yang T, *et al.* (2010): Brain volume alteration and the correlations with the clinical characteristics in drug-naïve first-episode MDD patients: A voxel-based morphometry study. *Neurosci Lett* 480:30–34.
75. Maller JJ, Daskalakis ZJ, Fitzgerald PB (2007): Hippocampal volumetrics in depression: The importance of the posterior tail. *Hippocampus* 17:1023–1027.
76. Videbech P, Ravnkilde B (2004): Hippocampal volume and depression: A meta-analysis of MRI studies. *Am J Psychiatry* 161:1957–1966.
77. Haldane M, Cunningham G, Androutsos C, Frangou S (2008): Structural brain correlates of response inhibition in bipolar disorder I. *J Psychopharmacol* 22:138–143.
78. Ito H, Kawashima R, Awata S, Ono S, Sato K, Goto R, *et al.* (1996): Hypoperfusion in the limbic system and prefrontal cortex in depression: SPECT with anatomic standardization technique. *J Nucl Med* 37:410–414.
79. Ma N, Li L, Shu N, Liu J, Gong GL, He Z, *et al.* (2007): White matter abnormalities in first-episode, treatment-naive young adults with major depressive disorder. *Am J Psychiatry* 164:823–826.
80. Hayasaka S, Laurienti PJ (2010): Comparison of characteristics between region-and voxel-based network analyses in resting-state fMRI data. *Neuroimage* 50:499–508.
81. Zalesky A, Fornito A, Harding IH, Cocchi L, Yücel M, Pantelis C, Bullmore ET (2010): Whole-brain anatomical networks: Does the choice of nodes matter? *Neuroimage* 50:970–983.
82. Fornito A, Zalesky A, Bullmore ET (2010): Network scaling effects in graph analytic studies of human resting-state FMRI data. *Front Syst Neurosci* 4:22.
83. Sanabria-Diaz G, Melie-García L, Iturria-Medina Y, Alemán-Gómez Y, Hernández-González G, Valdés-Urrutia L, *et al.* (2010): Surface area and cortical thickness descriptors reveal different attributes of the structural human brain networks. *Neuroimage* 50:1497–1510.
84. Mataix-Cols D, Wooderson S, Lawrence N, Brammer MJ, Speckens A, Phillips ML (2004): Distinct neural correlates of washing, checking, and hoarding symptom dimensions in obsessive-compulsive disorder. *Arch Gen Psychiatry* 61:564–576.
85. Damoiseaux JS, Greicius MD (2009): Greater than the sum of its parts: A review of studies combining structural connectivity and resting-state functional connectivity. *Brain Struct Funct* 213:525–533.
86. Honey CJ, Sporns O, Cammoun L, Gigandet X, Thiran JP, Meuli R, Hagmann P (2009): Predicting human resting-state functional connectivity from structural connectivity. *Proc Natl Acad Sci U S A* 106:2035–2040.